CHEMISTRY OF MATERIALS
Cite This: Chem. Mater. 2018, 30, 1989−1997
Article
pubs.acs.org/cm

Light-Controlled Shrinkage of Large-Area Gold Nanoparticle Monolayer Film for Tunable SERS Activity

Xuefei Lu,[†,‡] Youju Huang,*[,‡,§,∥] Baoqing Liu,[†,‡] Lei Zhang,[‡,§] Liping Song,[‡,§] Jiawei Zhang,[‡,§] Afang Zhang,[†] and Tao Chen*[,‡,§]

[†]Department of Polymer Materials, College of Materials Science and Engineering, Shanghai University, Nanchen Road 333, Shanghai 200444, China

[‡]Key Laboratory of Marine Materials and Related Technologies, Zhejiang Key Laboratory of Marine Materials and Protective Technologies, Ningbo Institute of Material Technology and Engineering, Chinese Academy of Sciences, Ningbo 315201, China

[§]University of Chinese Academy of Sciences, 19A Yuquan Road, Beijing 100049, China

[∥]Max Planck Institute for Polymer Research, Ackermannweg 10, 55128 Mainz, Germany

Supporting Information

ABSTRACT: The two-dimensional (2D) monolayer gold nanoparticle (Au NP) film is of significant interest and importance in both fundamental and practical applications including optoelectronic devices, sensing, catalysis, and surface-enhanced Raman spectroscopy (SERS). Because of the weak physical interaction, the conventional monolayer Au NP film fabricated at the oil−water interface was unstable, easily breakable, and difficultly transferred. In the present work, we report on a simple and effective chemical cross-linking strategy at the air−water interface to achieve a large-scale monolayer gold nanoparticle film with intelligently tunable size of nanogaps, and excellent free-standing and easily transferable properties. In our strategy, acrylamide, a polymerizable molecule, was first modified on the surface of Au NPs for subsequent self-assembly into a monolayer film at the liquid−liquid interface. Through photopolymerization of acrylamide, a chemically cross-linked film was formed with closely packed nanoparticles, highly macroscopic uniformity, and excellent free-standing property, which allowed it to be easily transferred from the air−water interface onto various solid substrates while maintaining its integrity. It is interesting to find that the macroscopic film underwent an *in situ* shrinkage under irradiation of UV-light, and its area shrinkage ratio is close to 55% (equal to 2.2 times) of that from non-cross-linked counterparts. More importantly, UV-light-controlled *in situ* shrinkage of the Au NP film would lead to intelligently, precisely tuned nanogaps less than 0.5 nm between neighboring Au NPs for maximal amplification of SERS signals, and the macroscopic uniformity of the films ensured the reproducible performance of SERS signals, providing an ideal candidate for SERS applications.

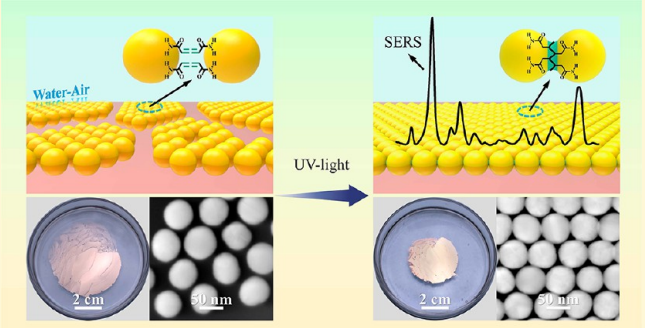

INTRODUCTION

Self-assembly of gold nanoparticles (Au NPs) into a two-dimensional (2D) monolayer film is a matter of interest from both fundamental and applicative standpoints. Because of the synergistic effect such as quantum confinement in discrete nanoparticles and interparticle coupling,[1−4] 2D Au NP monolayer films usually display unique physical and chemical properties that are quite different from those of either single nanoparticles or their bulk material counterparts, and are employed in various fields including optoelectronic devices,[5−7] optothermal devices,[8,9] catalysis,[10−12] sensors,[13,14] and surface-enhanced Raman scattering (SERS) spectroscopy.[15−17] Among them, the application for SERS gains much attention because of its advantage of fully utilizing the property of 2D plasmonic materials, which inherently generate intense localized electromagnetic fields and coupling between metallic NPs. It is well-known that small nanogaps, called "hot spots", result in a large Raman enhancement factor (EF) for single-molecule detection due to the ability of identifying the vibrational signature of target molecules.[18] On one hand, it is essential to control the size of nanogaps as well as the interaction between adjacent metallic NPs in the film for maximal amplification of SERS signals.[15,19,20] Jiang et al. have reported the fabrication of Au NP self-assembly monolayer films (SAMs), with uncovered and clean sub-1 nm gaps in high density, and used as SERS substrates.[15] Although the obtained films could generate a remarkable SERS performance for Raman scattering enhancement, a small fraction of voids still existed over the films

Received: December 14, 2017
Revised: March 6, 2018
Published: March 7, 2018

DOI: 10.1021/acs.chemmater.7b05176
Chem. Mater. 2018, 30, 1989−1997

because of repulsion and attractive van der Waals interaction between NPs.[21] On the other hand, from the perspective of a practical standpoint, highly macroscopic uniformity of films would ensure reproducible performance of SERS signals. Therefore, it is highly important to simultaneously precisely control the size of nanogaps, providing high-density nanogaps, and macroscopic uniformity of films with a smaller fraction of voids.

Recently, many research efforts have therefore been devoted to control over macroscopic uniformity of the film and SERS performance, including Langmuir−Blodgett compression,[22] addition of promoter,[23] and surface modification.[24] Although compression of SAMs with increased surface pressures at the interface is gifted at fabricating a closer packing of Au NPs, it is virtually noncovalent, resulting in a fragile property, and easily fractured when the films were transferred onto solid substrates.[24,25] More recently, Bell et al. put forward a method for promoting assembly of metallic and nonmetallic NPs into interfacial monolayer films using promoter added into the oil phase to reduce Coulombic repulsion between the particles,[23] but it seems to lack the ability of the preparation of large-area free-standing monolayer films. Marcin et al.[26] and Lin et al.[25] have synthesized a free-standing cross-linking monolayer of covalently bonded Au NPs; however, a complicated process for preparation of alkylthiol molecules and cross-linking agents as well as cumbersome catalysts are essential to form two-dimensional monolayer films. Despite this great progress, intelligent control over macroscopic uniformity of 2D Au NP films with dense and precisely size-controlled nanogaps for high and reproducible performance of SERS signals has remained quite challenging.

Herein, we describe a facile and effective synthesis of large-area SAMs fabricated via interfacial self-assembly of Au NPs with assistance of photoinitiation polymerization of the acrylamide ligand at the air−water interface. Unlike the conventional 2D Au NP films, photoinitiation interfacial polymerization-induced chemical cross-linking exhibits three distinctive properties. First, cross-linking of adjacent NPs resulted in a high mechanical strength of the film, making it unbreakable, free-standing, and easily transferred onto any solid substrates (plastic mold, PDMS, copper grid, silicon wafer, as well as filter paper). Second, interfacial polymerization led to the remarkable shrinkage of the 2D Au NP film, making the film much more macroscopically uniform and compressed, ultimately improving the density of nanogaps. Third, UV-light-dependent *in situ* shrinkage of Au NP films would provide a strategy to intelligently tune the size of nanogaps as well as macroscopic uniformity of the film for an ideal SERS candidate and for smart SERS devices or SERS-based applications.

EXPERIMENTAL SECTION

Materials. Gold(III) chloride trihydrate ($HAuCl_4{\cdot}3H_2O$, ≥49.0%) was bought from Sigma-Aldrich. Trisodium citrate dehydrate (SC, ≥99.0%), tris(hydroxymethyl)aminomethane (TB, GR), and *n*-hexane (GR) were obtained from Sinopharm Chemical Reagent Co., Ltd. (Shanghai, China). The 2-hydroxy-4′-(2-hydroxyethoxy)-2-methylpropiophenone (I-2959, 99%) was purchased from J&K SCIENTIFIC Co., Ltd. (Beijing, China). The 4-aminothiophenol (4-ATP, 97%) was purchased from Energy Chemical. Acrylamide (AAm, GR) and ethanol absolute (GR, 99.8%) were obtained from Aladdin. All chemicals were used as received without further purification. We used deionized water in all aqueous solutions. All glassware was cleaned using freshly prepared aqua regia (HCl/HNO_3 in a 3:1 ratio by volume) followed by rinsing with copious amounts of water.

Synthesis of Au NPs. Synthesis of Au NPs with diameters of 50 nm was according to our reported method.[27] In detail, 10 mL of SC (33 mM) solution was added into 140 mL of deionized water with continuous heating for 15 min and vigorous stirring as the temperature of the oil bath was at 100 °C. Then, 1 mL of fresh $HAuCl_4$ (25 mM) and 5 mL of TB (0.1 M) solution were sequentially added (time delay 60 s) until the temperature of the oil bath was at 137 °C. After 20 min of continuous heating, the temperature of the oil bath was maintained at 100 °C. Then, 1 mL of $HAuCl_4$ (25 mM) was injected an additional two times (interval of 30 min) to improve the shape and size uniformity of the particles. By changing the time or temperature of heating SC, it becomes possible to acquire different particle sizes.

Synthesis of Au NRs. Synthesis of Au NRs was according to a previous reported method.[28,29]

Functionalization of Au NPs with Acrylamide Ligands. The as-synthesized Au NPs (15 mL) were concentrated by centrifuging at 4500*g* for 10 min. After that, the supernatant was removed, and the residue was redispersed in H_2O (total volume is 15 mL). The solution was allowed to stir slowly for 12 h after acrylamide (1 mL, 7 μg/mL in water) and I-2959 (1 mL, 70 ng/mL in water) were added.

Light-Controlled Shrinkage of Au NPs at the Air−Water Interface by UV-Light. Self-assembly of Au NPs at the air−water interface was prepared according to a traditional method with some modifications.[15,24] In detail, 15 mL of Au NP solution modified with acrylamide was transferred to a glass culture dish (9 cm in diameter), and diluted with 8 mL of deionized water to fully cover the bottom of the culture dish, and 15 mL of hexane was added to the surface of the aqueous solution to form an immiscible water−hexane interface. A 10 mL portion of ethyl alcohol was then added dropwise to the surface of the water−hexane layers (0.6 mL/min, using a mechanical syringe pump), which led to Au NPs being trapped at the interface, as seen in Figure S12 (Supporting Information). Then, UV-light (wavelength of 365 nm, power of 15 mW/cm^2) was used to narrow the area of the Au NP monolayer film after complete volatilization of hexane. The process of irradiation was continued from 0 to 10 min.

Sample for Raman Tests. The Si-wafer-supported Au NP films were immersed into 2 mL of 1×10^{-4} M 4-ATP ethanol solution for 6 h and then rinsed repeatedly with water and ethanol to remove any surface residue.[30]

Spectroscopic, SERS, and Structural Characterization. UV−vis absorption spectra were recorded by virtue of a TU-1810 UV−vis spectrophotometer provided by Purkinje General Instrument Co., Ltd. ζ potential measurements were made by Malvern Instruments Co., Ltd. The morphologies of Au NPs were observed by an S-4800 (Hitachi, Japan) field emission scanning electron microscope (SEM) at an acceleration voltage of 4 kV. Transmission electron microscopy (TEM) was performed on a JEOL JEM 2100 electron microscope operating at 200 kV. Raman spectra were collected on an R-3000HR spectrometer (Raman Systems, Inc., R-3000 series) using a red LED laser (785 nm). Laser power was 0.5% (1.4 mW), and the focal diameter was around 1277 nm for all spectra. SERS spectra were collected using a 50× objective (Olympus) with a numerical aperture of 0.75 and an accumulation time of 10 s.

RESULTS AND DISCUSSION

Fabrication of Large-Area Gold Nanoparticle Monolayer Film. A coreduction tactic was used to synthesize monodispersed gold nanoparticles with a narrow size distribution (RSD ∼ 4−7%), using sodium citrate and tris-base as reducing agents as described in our previous work.[27] Then, the synthesized Au NPs were employed for self-assembly into a large-area monolayer film at the water−hexane interface. Briefly, *n*-hexane was carefully added into the Au NP solution to form an oil−water interface between two immiscible liquids. Subsequently, ethanol was slowly added dropwise, which results in a sharp decrease of Au NP surface charge, thus driving the trap of Au NPs at the interface.[15,21,31] Figure S1 (Supporting Information) shows typical images of the self-assembly

DOI: 10.1021/acs.chemmater.7b05176
Chem. Mater. 2018, 30, 1989−1997

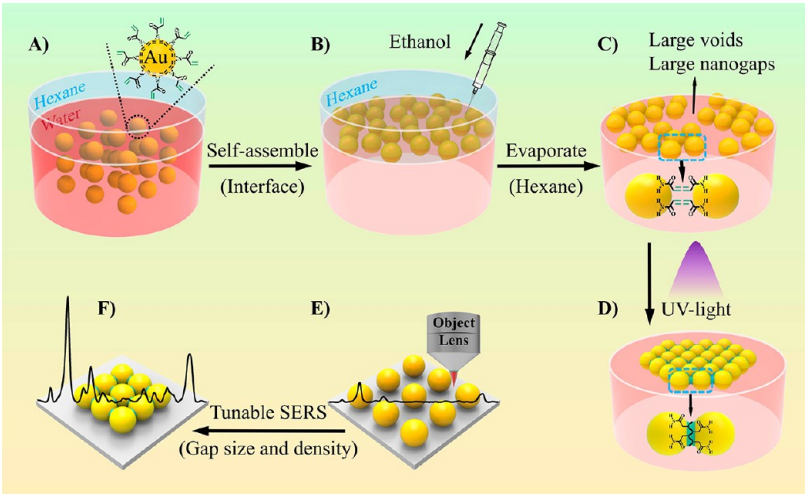

Figure 1. Schematic illustration of shrinkable Au NP monolayer films induced by interfacial cross-linking at the air−water interface. (A) The hexane was carefully introduced in the aqueous solution of acrylamide-modified Au NPs for formation of an immiscible interface. (B) The interface trapped Au NPs by addition of ethanol as an inducer. (C) Evaporation of hexane resulted in SAMs with large voids and large nanogaps between NPs. (D) Light-controlled shrinkage and cross-linking of SAMs. (E, F) The SAMs transferred onto silicon wafers for tunable SERS via changing the size and density of nanogaps.

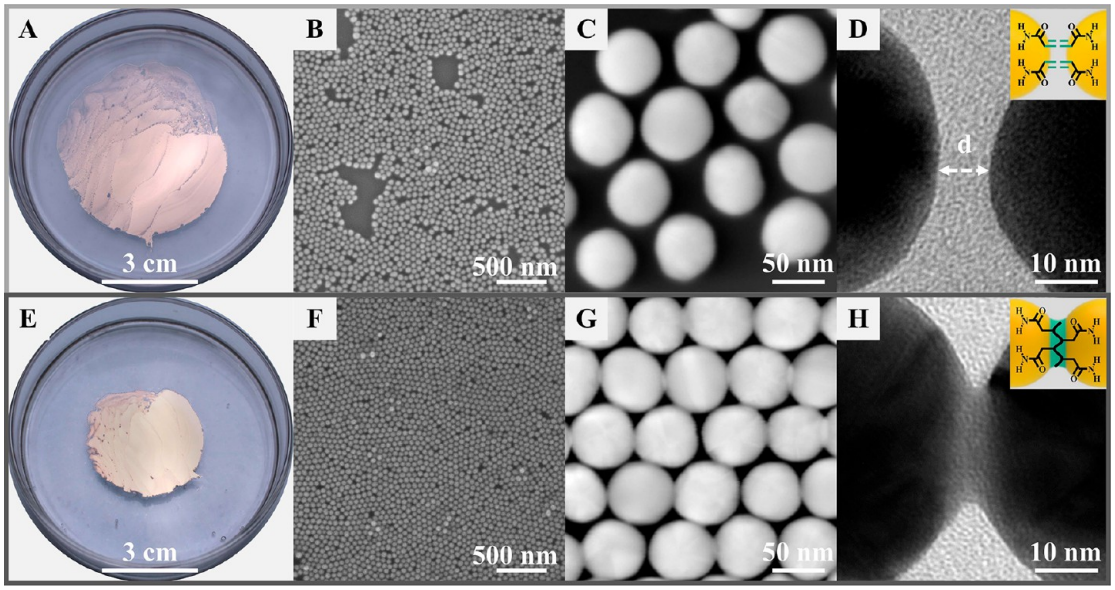

Figure 2. Optical, SEM, and TEM images of large-area cross-linked monolayer films. The optical images of SAMs fabricated at the interface possess an area of (A) ~21.6 cm^2, and (E) ~9.7 cm^2 obtained by statistically measuring the zone within the dashed lines. SEM and TEM images of Au NP SAMs (B−D) before and (F−H) after irradiation of UV-light. (H) Typical linkage structure shown in magnification view.

monolayer films (SAMs). Although this approach has been widely used to form large-area monolayer films, inhomogeneous microscopic features and a large number of voids were often observed in the resultant films,[32,33] possibly because of the long-range, particle−particle repulsion force due to residual charge on the Au NP surface.[21]

To fabricate large-area SAMs with fewer voids and more uniformity, we introduced acrylamide molecules modified on the surface of Au NPs and then self-assembled into a monolayer film at the hexane−water interface as shown in Figure 1A,B. The acrylamide (AAm) molecule can interact with citrate-capped Au NPs via the coordination bonding between Au and NH_2.[13] Compared with the conventional interfacial SAMs, introduction of acrylamide molecules before interfacial self-assembly shows distinctive advantages. First, functionalization of acrylamide molecules on the surface of Au NPs significantly decreases the residual electrostatic charge as testified by the ζ potential in Figure S2 (Supporting Information), which greatly improves the uniformity and size of the resultant films. The optical image (Figure 2A) of SAMs shows a large area of ~21.6 cm^2. Scanning electron microscopy (SEM) and transmission electron microscopy (TEM) measurements indicated the resultant films with a small fraction of voids and around 5 nm nanogaps among NPs as shown in Figure 2B−D and Figure S3A (Supporting Information). Second, it is well-known that capillary and van der Waals forces (green arrows), electrostatic and steric repulsion (purple arrows), and solvation and line tension (red arrows) between NPs play a key role in the formation of a monolayer at the water−oil interface,[13,21] as shown in Figure S4 (Supporting Information).

DOI: 10.1021/acs.chemmater.7b05176
Chem. Mater. 2018, 30, 1989−1997

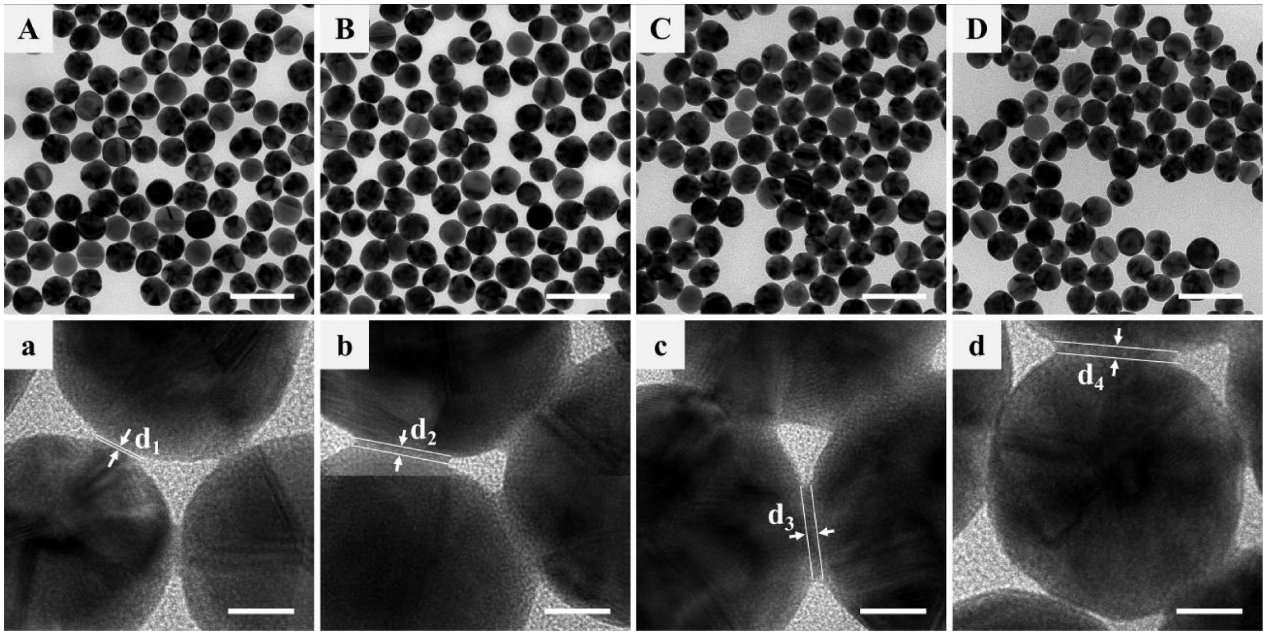

Figure 3. Different dosage of acrylamide monomer. The molar ratio of acrylamide ligand to Au NPs from (A) 10^4:1 to (B) 10^5:1, (C) 10^6:1, and to (D) 10^7:1, respectively. The bottom row shows magnification images corresponding to the top row. The scale bars in parts A–D and a–d represent 100 and 10 nm, respectively.

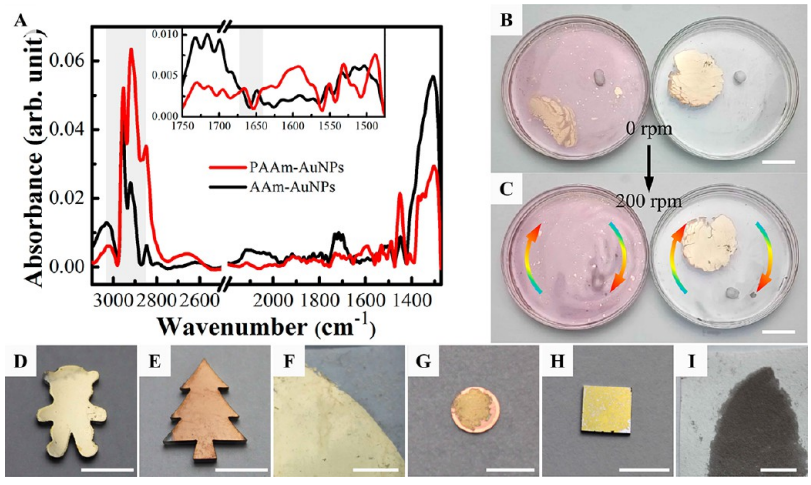

Figure 4. Demonstration of mechanical properties of Au NP SAMs after cross-linking. (A) Fourier transform attenuated total reflection infrared spectrometry (FTIR-ATR) of Au NP SAMs before (AAm-Au NPs) and after (PAAm-Au NPs) irradiation. (B, C) Successive stages of deformed films were stirred at different speeds. Photos of the self-assembled films transferred to different substrates: (D, E) plastic molds, (F) PDMS, (G) copper grid, (H) silicon wafer, and (I) filter paper. The scale bars are 1 cm (D, E, I), 5 mm (F, H), and 3 mm (G).

The introduction of acrylamide molecules provides the double bonds for polymerization and cross-linking of adjacent NPs, which would remarkably avoid the numerous physical interactions to equilibrate the repulsive interaction and attractive interaction with respect to the conventional interfacial self-assembly.[26] We carried out the polymerization of the acrylamide ligand under irradiation of UV-light and existence of photoinitiator (I-2959), shown in Figure 1C,D. It is very interesting to find that SAM after irradiation shows a significant area shrinkage decreased to ~9.7 cm^2 (Figure 2E) from ~21.6 cm^2 (Figure 2A) before irradiation. Its area shrinkage ratio is ~54.9% (equal to 2.2 times) of that for the non-cross-linked case. The area shrinkage ratio is calculated using the following equation: $\eta = (S_{before} - S_{after})/S_{after} \times 100\%$, where S_{before} and S_{after} represent the area of SAMs before and after irradiation by UV-light, respectively. The proportion of voids and size of nanogaps were less than 0.3% and 0.5 nm [relative standard deviation (RSD) of ~15%], respectively, as shown in Figure 2F–H and Figure S3B (Supporting Information). It is hard to find large voids, and a near hexagonal local arrangement of Au NPs is revealed. At the same time, the SAMs' color changed from rose gold to gold. Furthermore, the typical linkage or "glue" structure is shown in Figure 2G–H compared with the non-cross-linked condition (Figure 2C,D), which provides evidence that the polymerization has successfully cross-linked Au NPs at the interface.

To explore the universality of the present approach of light-induced interfacial cross-linking among Au NPs, we tested a series of molecules. It was found that only molecule, with one functional group for interaction with Au NPs and another

DOI: 10.1021/acs.chemmater.7b05176
Chem. Mater. 2018, 30, 1989–1997

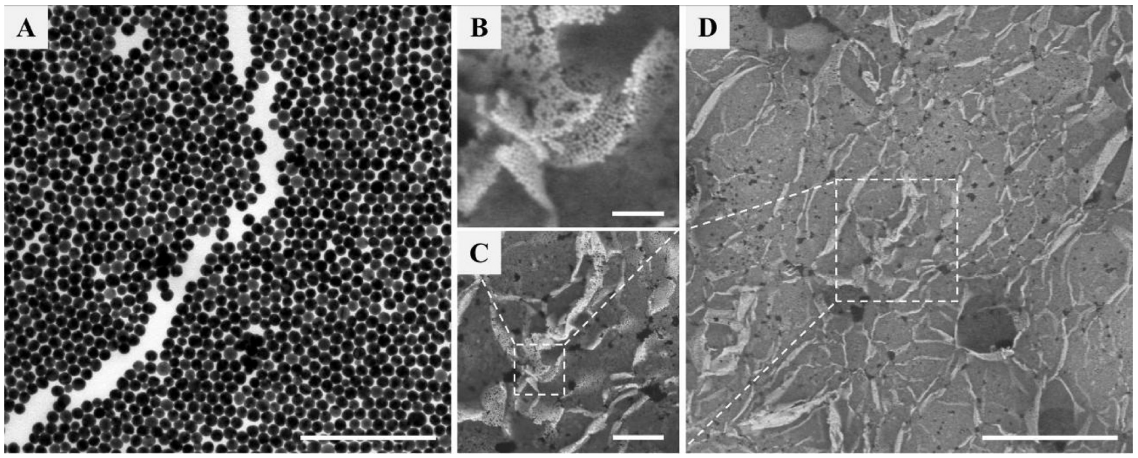

Figure 5. Demonstration of mechanical properties of Au NP SAMs after cross-linking. (A) Shape of the crack indicating that the film broke in a way characteristic of a solid. (B–D) Different magnification of SEM images presents a turn-up configuration on the edge of films composed of the cross-linked Au NPs. The scale bars are 500 nm (A, B), 2 μm (C), and 10 μm (D).

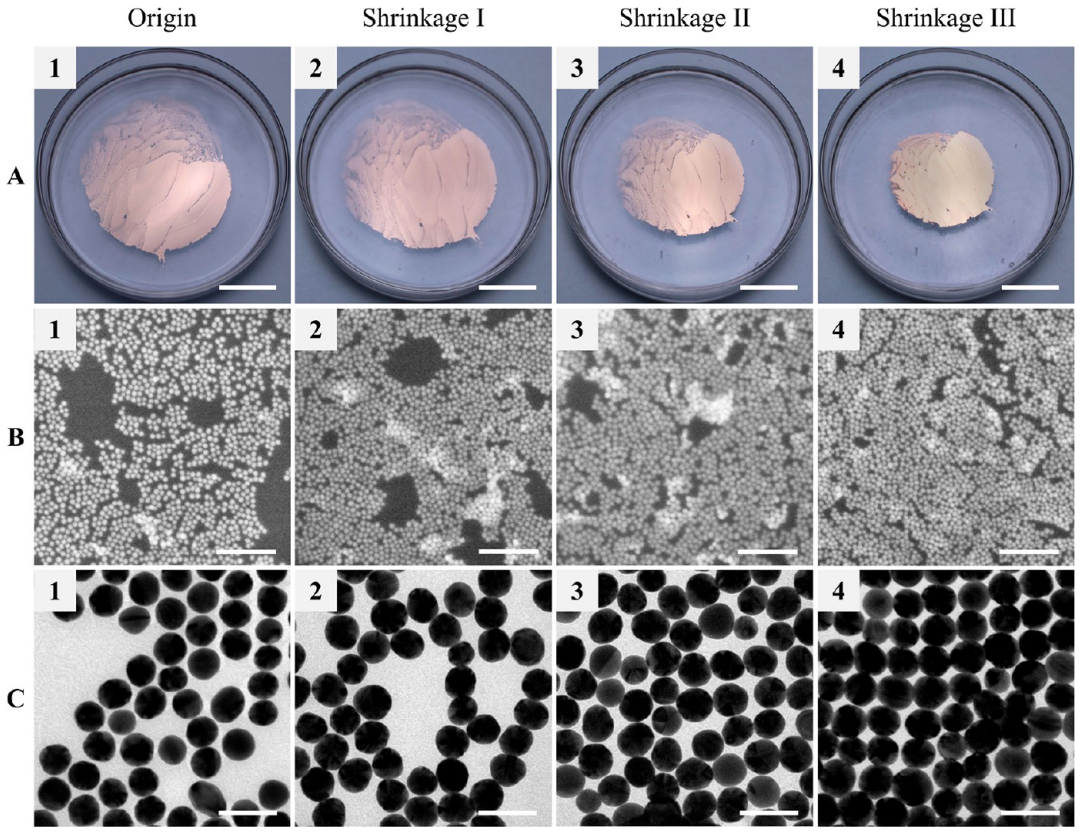

Figure 6. Optical, SEM, and TEM photos of gradually increased irradiation time with 0 min (Origin), 2 min (Shrinkage I), 5 min (Shrinkage II), and 10 min (Shrinkage III) by UV-light. The scale bars are 2 cm (A), 500 nm (B), and 100 nm (C).

functional group for cross-linking or polymerization, could achieve the light-induced interfacial cross-linking monolayer Au NP film. Thus, the molecule with a group of C═C bond and another group of NH_2, COOH, OH, and CH_3, such as 2-aminoethyl methacrylate (AEMA), acrylic acid (AAc), 2-hydroxyethyl methacrylate (HEMA), and *N*-isopropylacrylamide (NIPAM), were employed. Keeping the same mole ratio of acrylic molecules to Au NPs (10^5:1), the self-assembled film at the air–water interface was irradiated by UV-light for 15 min. TEM images show the microcosmic phenomena of the film in Figure S5 (Supporting Information). Au NPs modified with AEMA, AAc, and HEMA could form the typical linkage or "glue" structure as shown in Figure 2H, while the molecule with only the C═C bond such as NIPAM could not achieve the microcosmic cross-linking. In addition, the dosage of ligand and photoinitiator is also a key factor to directly affect the cross-linking area and nanogap between neighboring NPs. We investigated the effect by cross-linking Au NPs with mole ratio from 10^4:1 to 10^5:1, 10^6:1, and to 10^7:1 as shown in Figure 3. The cross-linking area and nanogap ($d_1 < d_2 < d_3 \approx d_4$) became bigger with the concentration increase of acrylamide, which

DOI: 10.1021/acs.chemmater.7b05176
Chem. Mater. 2018, 30, 1989–1997

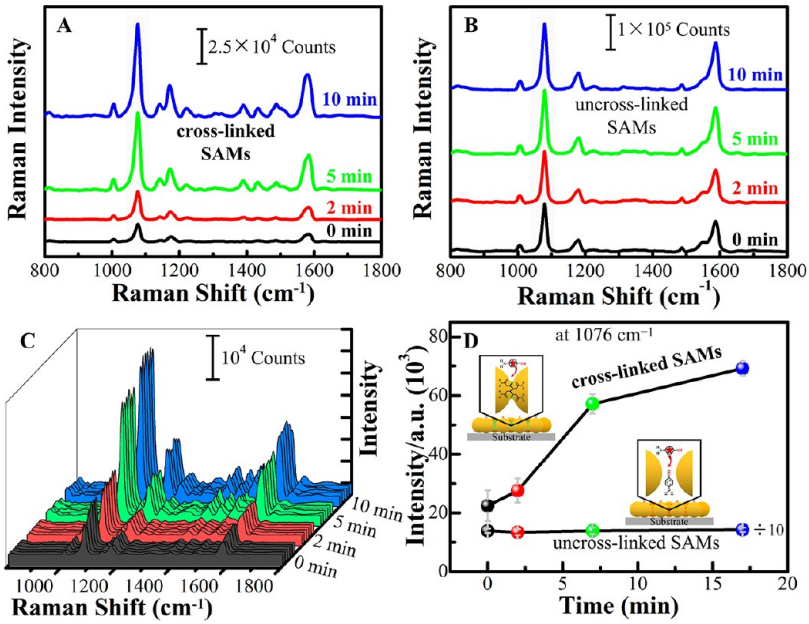

Figure 7. Tunable SERS activities. Raman spectra of (A) cross-linked Au NP SAMs and (B) un-cross-linked ones with gradually increased irradiation time for 0 min (black line), 2 min (red line), 5 min (green line), and 10 min (blue line) by UV-light. The exposure time was 10 s, laser wavelength was 785 nm, and laser power was 1.4 mW. (C) SERS spectra of 4-ATP (10^{-4} M) acquired from 5 random sites of cross-linked SAMs with different irradiation times. (C) Schematic illustration of different types of Au NP SAMs transferred onto the substrate for Raman tests. (D) Plot of SERS intensity from peak 1076 cm^{-1} and the maximum absorption peak versus the time of irradiation. The standard deviations are averaged from 10 individual experiments.

may be due to many more molecules being used to polymerize and cross-link between adjacent NPs.

High-Performance Free-Standing Films. The ligand of acrylamide was immobilized on the citrate-capped Au NP surface via coordination bonds between Au and NH_2, and electrostatic interactions between the carboxyl groups of the citrate ligand and the amino groups of AAm.[13,34] The inherent change of Au NPs is that the C═C bond could achieve the polymerization of acrylamide ligands after irradiation of UV-light. The Fourier transform attenuated total reflection infrared spectrometry (FTIR-ATR) of Au NP SAMs was recorded (Figure 4A). The C═C and C═O stretching vibrations (ν(C═C) and ν(C═O)) of AAm show an overlap around 1680−1630 cm^{-1}. It is hard to distinguish the change after polymerization of the C═C bond from this region. Furthermore, the unsaturated CH_2 stretching vibrations ($\nu(CH_2)$ of 3033 cm^{-1}) were observed, revealing that molecules of AAm were modified on the surface of Au NPs. After light-initiated polymerization, the intensity of the characteristic peak of $\nu(CH_2)$ faded away. At the same time, the characteristic peaks of saturated CH_2 stretching vibrations ($\nu(CH_2)$) were distinct at 2920 and 2850 cm^{-1}. The peak at 2953 cm^{-1} may arise from CH_3 stretching vibrations. FTIR-ATR results indirectly confirmed that AAm molecules were successfully polymerized and cross-linked in Au NP SAMs.

For easily distinguishing the mechanical property of the film, the obtained contractive Au NP SAMs induced by interfacial cross-linking have a comparative study as shown in Figure 4B,C and Movie S1. When the film was floating on the surface of water, magnetic stirring of the solution using a stir bar was employed. It is clear to see that the non-cross-linked film tends to break into small pieces and finally disappeared, while the cross-linked film can tolerate critical deformation under robust external force until the speed increased up to 200 rpm, with only a little crack appearing. Additionally, the non-cross-linked film usually breaks when transferred onto substrates. The cross-linked film can be easily transferred onto different substrates, such as plastic molds, PDMS, copper grids, silicon wafer, and filter paper, while maintaining its integrity, as shown in Figure 4D−I, which would broaden its application to various fields.

For further characterization of the freestanding performance of the film, the obtained cross-linked Au NP films were studied with the aid of TEM and SEM after the film. Figure 5A shows a crack in the monolayer film caused by mechanical stress during the transfer process, displaying characteristic features of stiff materials of the sharp matching edges. Such a crack shape indicates that the film broke in a way characteristic of a solid. This further confirmed that the Au NPs within the film are linked through chemical bonds.[26] It should be noted that, importantly, the magnified SEM image in Figure 5B−D presents a turn-up configuration on the edge of films composed of the cross-linked Au NPs. Such a turn-up configuration and plenty of crinkling shapes in the film directly confirmed that the cross-linked monolayer shows high performance of the free-standing film.

Dynamically Tuning the Shrinkage and Cross-Linking of the Au NP SAMs. Figure 6 shows representative optical, SEM, and TEM images obtained as a function of time by UV-light irradiation. There were 2D arrays of Au NPs with relatively large voids and inter-nanogaps when no UV-light (origin) was applied (shown in Figure 6B,C, Figure 2A−D). The domain of the closely packed Au NPs in the TEM images also shows large void areas in previous reports.[15,24] Since the SAMs are very stable at the interface, the entrapped NPs at the interface should retain a certain electrostatic repulsive force preventing the generation of closely packed aggregation by counteracting the van der Waals interaction. In fact, the observed voids of SAMs were usually inevitable, which results

DOI: 10.1021/acs.chemmater.7b05176
Chem. Mater. 2018, 30, 1989−1997

in macroscopic nonuniformity and impedes practical applications.[33] Optical microscope images were acquired by gradually increasing irradiation time with 2 min (Shrinkage I), 5 min (Shrinkage II), and 10 min (Shrinkage III) by UV-light with power of 250 W and wavelength of 365 nm. The color of the SAMs gently changed from rose gold to gold, showing tunable optical properties, even electrical properties.[35,36] Additionally, their area shrinkage ratios of the cross-linked films at the diverse compressed stages shown in Figure 6A are approximately 2.4%, 33.1%, and 54.9% of that of the non-cross-linked case, respectively. The maximum of area shrinkage ratio is around 55.1%, and more irradiation time would not lead to further shrinkage. Figure 6B,C shows the microcosmic change of films, indicating that the voids gradually decreased and finally disappeared, which plays a dominating role for the decreased area of SAMs. It is noteworthy that, after irradiation, the nanogaps between adjacent NPs gradually decrease and are less than 0.5 nm (Figure 6C and Figure 2H). This means that the intensive shrinkage maybe provides the opportunity for immediate cross-linking of NPs via the C═C double bond of acrylamide molecules and prevents reseparation because of more and more cross-links between adjacent NPs. The effect of the irradiation on shrinkage of the SAMs is remarkable and effectively overcomes the drawback of the films self-assembled at the interface with higher homogeneity and free-standing performance.

Tunable SERS Efficiency. For an understanding of the cover of PAAm (polyacrylamide) on the surfaces of Au NPs, an EDS (energy-dispersive spectroscopy) elemental mapping of interfacial cross-linked Au NP films was recorded (Figure S6). Light blue (B), green (C), red (D), orange (E), and yellow (F) colors represent Au, S, C, N, and O element, respectively. It is clear to see that PAAm is covered on the surface and in the nanogaps of Au NPs from the distribution of C, N, and O element in Figure S6D−F and FTIR in Figure 4A. Notably, on one hand, the molar ratio of acrylamide ligand to Au NPs was 10^5:1 in Figure 2B, approximately equal to the monolayer absorbance of the acrylamide ligand on the surface of a gold nanoparticle. This means that polymerization of the acrylamide ligand would not form a compact polymer network and hinder the availability of the target molecules into the nanogap. On the other hand, sulfur element (S) was only acquired after immersion into the solution of model Raman analyte of 4-aminothiophenol (4-ATP). In Figure S6C, the S element was clearly dispersed in between nanogaps and on the surface of Au NPs as in contrast with C, N, and O element, which indirectly confirmed that the 4-ATP molecule is available at the nanogaps.

For evaluation of the SERS activity of the light-controlled shrinkage of large-area Au NP SAMs, 4-aminothiophenol (4-ATP) was used as a model Raman analyte to investigate the effect of SAM shrinkage on SERS performance as shown in Figure 1E,F. It is clearly known that different irradiation times of Au NP SAMs under UV-light would lead to a different degree of shrinkage. Therefore, four samples with different irradiation times were immersed into 2 mL of 10^{-4} M 4-ATP solution for SERS detection at a 785 nm excitation wavelength.

Figure 7A shows the recorded SERS spectra of 4-ATP, dominated by a set of peaks located at 1076, 1172, and 1578 cm^{-1} corresponding to the mixed modes of C−C stretching and C−S stretching; C−H in-plane, bending vibration; and parallel C−C stretching vibration, respectively. The characteristic peaks of the 4-ATP molecule are in good agreement with previous reports.[15] Among them, the strong fingerprint vibrational band at 1076 cm^{-1} was selected to calculate the enhanced factors (EFs; see the Supporting Information for sample EFs calculation).[37] Interestingly, we found that EFs were directly related to the shrinkage ratio of films irradiated by UV-light. The EFs of the films can be calculated using the following equation:[37] $EF = \frac{N_{bulk} I_{surf}}{N_{surf} I_{bulk}}$, where N_{bulk} and N_{surf} represent the number of 4-ATP molecules in the bulk solid sample and on the surface of the Au NP films, respectively; and I_{bulk} and I_{surf} denote the Raman scattering intensities from the solid 4-ATP and the 4-ATP adsorbed on surface of the Au NP films. On the basis of the measured values, EF values gradually increased with increasing irradiation time until the maximum EF value reaches 7×10^7 within 17 min (Supporting Information). With the increased irradiation time, Raman intensity and absorbance peak of SAMs are all gradually increased as shown in Figure 7A,C and Figure S7 (Supporting Information), which show the same variation trend and tunable SERS activity. It is noted that the RSD (relative standard deviation) of Raman intensity at 1076 cm^{-1} is gradually decreased from 22.1% to 15.4%, 8.5%, and to 5.6% by changing the irradiation time, which means more reliable repeatability and practicability. In Figure S7 (Supporting Information), the absorption peaks of films transferred onto thin PDMS substrates gradually ascended from 763 to 771, 780, and to 787 nm and approached the wavelength of laser light (785 nm) for maximal overlapping and amplification of SERS signals due to smaller inter-nanogaps and stronger coupling interaction between NPs,[38] because EF is usually obtained when the plasmonic resonance band matches closely the excitation laser wavelength.[39]

It is also found that there is a slight difference of SERS spectra between Figure 7A and Figure 7B, which may be ascribed to two aspects. One is spectral characteristic peaks caused by dimerization of 4-ATP. The other is spectral intensity enhanced by the charge transfer (CT) resonance between metal and 4-ATP. For confirmation of this issue, Raman spectroscopic investigation was conducted. On one hand, original Raman spectra of cross-linked Au NP SAMs with gradually increased irradiation time were normalized in Figure S8. It shows no obvious change at characteristic peaks of R—N═N—R (the peak intensities at 1142 cm^{-1} associated with C—N stretching mode, and at 1390 and 1436 cm^{-1} associated with N═N stretching vibration mode of 4,4′-dimercaptoazobenzene, which indicated the conversion from 4-ATP into DMAB).[15] In other words, the plasmon-driven catalytic efficiency of dimerization of 4-ATP seems to change as irradiation time increased. Additionally, the probe molecule of 4-methylthiobenzoic acid (4-MBA) also has a similar result as shown in Figure S7, which possesses an accompanying increase in Raman signal intensity but no dimerization reaction. Therefore, it can be attributed to the intrinsic CT resonance between metal and 4-ATP rather than dimerization of 4-ATP for the spectral change in intensity (shown in Figure 7A).

The probe molecule of 4-methylthiobenzoic acid (4-MBA) also shows a similar SERS activity as shown in Figure S9 (Supporting Information). The shrinkage of Au NP SAMs results in the increase of SERS signals and can be ascribed to the increase of the hotspot density and the decreased size of nanogaps between adjacent NPs, which inherently generate strong coupling and highly reproducible SERS activity.[40] We also measured the Raman efficiency of differently sized Au NPs and gold nanorods (Au NRs) under the same experimental

DOI: 10.1021/acs.chemmater.7b05176
Chem. Mater. 2018, 30, 1989−1997

conditions (Figures S10 and S11, Supporting Information). The strategy of light-controlled shrinkage of SAMs has universality for diversely sized and shaped metal NPs with tunable wavelength and photothermal effect, which display an excellent platform for monitoring of dynamic SERS performance.

CONCLUSION

We have demonstrated that introduction of polymerizable molecules in interfacial self-assembly can achieve the successful chemical cross-linking of a monolayer gold nanoparticle film, which provides a simple, general, and effective strategy to fabricate highly macroscopically uniform and excellent free-standing monolayer nanoparticle films. The macroscopic film underwent an *in situ* shrinkage under irradiation of UV-light, resulting in a gradual decrease of the area of the Au NP film. This would easily, precisely tune the uniformity of the macroscopic film and nanogaps between adjacent Au NPs, providing an ideal and smart candidate for various applications, such as SERS substrates, sensors, and photothermal and photoelectronic devices.

ASSOCIATED CONTENT

Supporting Information

The Supporting Information is available free of charge on the ACS Publications website at DOI: 10.1021/acs.chemmater.7b05176.

Photographs, UV−vis spectra, ζ potential, TEM and SEM micrographs, and normal Raman spectra (PDF)

Movie S1: Demonstration of the mechanical property of the film stirred at the air−water interface (AVI)

AUTHOR INFORMATION

Corresponding Authors

*E-mail: huangyouju@mpip-mainz.mpg.de.

*E-mail: tao.chen@nimte.ac.cn.

ORCID

Youju Huang: 0000-0001-5815-9784

Jiawei Zhang: 0000-0002-3182-9239

Afang Zhang: 0000-0002-0078-3223

Tao Chen: 0000-0001-9704-9545

Notes

The authors declare no competing financial interest.

ACKNOWLEDGMENTS

We gratefully acknowledge the Natural Science Foundation of China (Grant 51473179), the Bureau of Frontier Science and Education of Chinese Academy of Sciences (QYZDB-SSW-SLH036), Fujian province-Chinese Academy of Sciences STS project (2017T31010024), and Youth Innovation Promotion Association of Chinese Academy of Science (2016268 and 2017337).

REFERENCES

(1) Ding, S. Y.; Yi, J.; Li, J. F.; Ren, B.; Wu, D. Y.; Panneerselvam, R.; Tian, Z. Q. Nanostructure-based plasmonenhanced Raman spectroscopy for surface analysis of materials. *Nat. Rev. Mater.* **2016**, *1*, 16021.

(2) Lee, Y. H.; Shi, W.; Lee, H. K.; Jiang, R.; Phang, I. Y.; Cui, Y.; Isa, L.; Yang, Y.; Wang, J.; Li, S.; Ling, X. Y. Nanoscale surface chemistry directs the tunable assembly of silver octahedra into three two-dimensional plasmonic superlattices. *Nat. Commun.* **2015**, *6*, 6990.

(3) Turek, V. A.; Cecchini, M. P.; Paget, J.; Kucernak, A. R.; Kornyshev, A. A.; Edel, J. B. Plasmonic Ruler at the Liquid-Liquid Interface. *ACS Nano* **2012**, *6*, 7789−7799.

(4) Guo, Q.; Xu, M.; Yuan, Y.; Gu, R.; Yao, J. Self-Assembled Large-Scale Monolayer of Au Nanoparticles at the Air/Water Interface Used as a SERS Substrate. *Langmuir* **2016**, *32*, 4530−4537.

(5) Fang, P. P.; Chen, S.; Deng, H. Q.; Scanlon, M. D.; Gumy, F.; Lee, H. J.; Momotenko, D.; Amstutz, V.; Salazar, F. C.; Pereira, C. M.; Yang, Z. L.; Girault, H. H. Conductive Gold Nanoparticle Mirrors at Liquid/Liquid Interfaces. *ACS Nano* **2013**, *7*, 9241−9248.

(6) Kim, J.; Son, D.; Lee, M.; Song, C.; Song, J. K.; Koo, J. H.; Lee, D. J.; Shim, H. J.; Kim, J. H.; Lee, M.; Hyeon, T.; Kim, D. H. A wearable multiplexed silicon nonvolatile memory array using nanocrystal charge confinement. *Sci. Adv.* **2016**, *2*, e1501101.

(7) Xu, Y. K.; Konrad, M. P.; Trotter, J. L.; McCoy, C. P.; Bell, S. E. J. Rapid One-Pot Preparation of Large Freestanding Nanoparticle-Polymer Films. *Small* **2017**, *13*, 1602163.

(8) Liu, Y.; Yu, S.; Feng, R.; Bernard, A.; Liu, Y.; Zhang, Y.; Duan, H.; Shang, W.; Tao, P.; Song, C.; Deng, T. A bioinspired, reusable, paper-based system for high-performance large-scale evaporation. *Adv. Mater.* **2015**, *27*, 2768−2774.

(9) Chen, Z.; He, S.; Butt, H. J.; Wu, S. Photon upconversion lithography: patterning of biomaterials using near-infrared light. *Adv. Mater.* **2015**, *27*, 2203−2206.

(10) Zhang, L.; Xiao, P.; Lu, W.; Zhang, J. W.; Gu, J. C.; Huang, Y. J.; Chen, T. Macroscopic Ultrathin Film as Bio-Inspired Interfacial Reactor for Fabricating 2D Freestanding Janus CNTs/AuNPs Hybrid Nanosheets with Enhanced Electrical Performance. *Adv. Mater. Interfaces* **2016**, *3*, 1600170.

(11) Smirnov, E.; Peljo, P.; Scanlon, M. D.; Girault, H. H. Interfacial Redox Catalysis on Gold Nanofilms at Soft Interfaces. *ACS Nano* **2015**, *9*, 6565−6575.

(12) Zhang, L.; Gu, J. C.; Song, L. P.; Chen, L.; Huang, Y. J.; Zhang, J. W.; Chen, T. Underwater superoleophobic carbon nanotubes/core−shell polystyrene@Au nanoparticles composite membrane for flow-through catalytic decomposition and oil/water separation. *J. Mater. Chem. A* **2016**, *4*, 10810−10815.

(13) Ding, T.; Rudrum, A. W.; Herrmann, L. O.; Turek, V.; Baumberg, J. J. Polymer-assisted self-assembly of gold nanoparticle monolayers and their dynamical switching. *Nanoscale* **2016**, *8*, 15864−15869.

(14) Wu, S.; Butt, H. J. Near-Infrared-Sensitive Materials Based on Upconverting Nanoparticles. *Adv. Mater.* **2016**, *28*, 1208−1226.

(15) Si, S. R.; Liang, W. K.; Sun, Y. H.; Huang, J.; Ma, W. L.; Liang, Z. Q.; Bao, Q. L.; Jiang, L. Facile Fabrication of High-Density Sub-1-nm Gaps from Au Nanoparticle Monolayers as Reproducible SERS Substrates. *Adv. Funct. Mater.* **2016**, *26*, 8137−8145.

(16) Chen, J.; Huang, Y.; Kannan, P.; Zhang, L.; Lin, Z.; Zhang, J.; Chen, T.; Guo, L. Flexible and Adhesive Surface Enhance Raman Scattering Active Tape for Rapid Detection of Pesticide Residues in Fruits and Vegetables. *Anal. Chem.* **2016**, *88*, 2149−2155.

(17) Huang, Y. J.; Dai, L. W.; Song, L. P.; Zhang, L.; Rong, Y.; Zhang, J. W.; Nie, Z. H.; Chen, T. Engineering Gold Nanoparticles in Compass Shape with Broadly Tunable Plasmon Resonances and High-Performance SERS. *ACS Appl. Mater. Interfaces* **2016**, *8*, 27949−27955.

(18) Nie, S. M.; Emory, S. R. Probing Single Molecules and Single Nanoparticles by Surface-Enhanced Raman Scattering. *Science* **1997**, *275*, 1102−1106.

(19) Lee, J. H.; Nam, J. M.; Jeon, K. S.; Lim, D. K.; Kim, H.; Kwon, S.; Lee, H.; Suh, Y. D. Tuning and Maximizing the Single-Molecule Surface-Enhanced Raman Scattering from DNA-Tethered Nanodumbbells. *ACS Nano* **2012**, *6*, 9574−9584.

(20) Nam, J. M.; Oh, J. W.; Lee, H.; Suh, Y. D. Plasmonic Nanogap-Enhanced Raman Scattering with Nanoparticles. *Acc. Chem. Res.* **2016**, *49*, 2746−2755.

(21) Reincke, F.; Hickey, S. G.; Kegel, W. K.; Vanmaekelbergh, D. Spontaneous assembly of a monolayer of charged gold nanocrystals at the water/oil interface. *Angew. Chem., Int. Ed.* **2004**, *43*, 458−462.

DOI: 10.1021/acs.chemmater.7b05176
Chem. Mater. 2018, 30, 1989−1997

(22) Nie, H. L.; Dou, X.; Tang, Z.; Jang, H. D.; Huang, J. High-Yield Spreading of Water-Miscible Solvents on Water for Langmuir-Blodgett Assembly. *J. Am. Chem. Soc.* **2015**, *137*, 10683−10688.
(23) Xu, Y. K.; Konrad, M. P.; Lee, W. W.; Ye, Z.; Bell, S. E. A Method for Promoting Assembly of Metallic and Nonmetallic Nanoparticles into Interfacial Monolayer Films. *Nano Lett.* **2016**, *16*, 5255−5260.
(24) Park, Y. K.; Yoo, S. H.; Park, S. Assembly of Highly Ordered Nanoparticle Monolayers at a Water/Hexane Interface. *Langmuir* **2007**, *23*, 10505−10510.
(25) Kosif, I.; Kratz, K.; You, S. S.; Bera, M. K.; Kim, K.; Leahy, B.; Emrick, T.; Lee, K. Y.; Lin, B. Robust Gold Nanoparticle Sheets by Ligand Cross-Linking at the Air-Water Interface. *ACS Nano* **2017**, *11*, 1292−1300.
(26) Andryszewski, T.; Iwan, M.; Hołdyński, M.; Fiałkowski, M. Synthesis of a Free-Standing Monolayer of Covalently Bonded Gold Nanoparticles. *Chem. Mater.* **2016**, *28*, 5304−5313.
(27) Lu, X. F.; Dandapat, A.; Huang, Y. J.; Zhang, L.; Rong, Y.; Dai, L. W.; Sasson, Y.; Zhang, J. W.; Chen, T. Tris base assisted synthesis of monodispersed citrate-capped gold nanospheres with tunable size. *RSC Adv.* **2016**, *6*, 60916−60921.
(28) Dai, L. W.; Song, L. P.; Huang, Y. J.; Zhang, L.; Lu, X. F.; Zhang, J.; Chen, T. Bimetallic Au/Ag Core-Shell Superstructures with Tunable Surface Plasmon Resonance in the Near-Infrared Region and High Performance Surface-Enhanced Raman Scattering. *Langmuir* **2017**, *33*, 5378−5384.
(29) Ye, X.; Zheng, C.; Chen, J.; Gao, Y.; Murray, C. B. Using binary surfactant mixtures to simultaneously improve the dimensional tunability and monodispersity in the seeded growth of gold nanorods. *Nano Lett.* **2013**, *13*, 765−771.
(30) Chen, Y.; Si, K. J.; Sikdar, D.; Tang, Y.; Premaratne, M.; Cheng, W. L. Ultrathin Plasmene Nanosheets as Soft and Surface-Attachable SERS Substrates with High Signal Uniformity. *Adv. Opt. Mater.* **2015**, *3*, 919−924.
(31) Shin, Y.; Song, J.; Kim, D.; Kang, T. Facile Preparation of Ultrasmall Void Metallic Nanogap from Self-Assembled Gold-Silica Core-Shell Nanoparticles Monolayer via Kinetic Control. *Adv. Mater.* **2015**, *27*, 4344−4350.
(32) Yang, G.; Hallinan, D. T. Gold Nanoparticle Monolayers from Sequential Interfacial Ligand Exchange and Migration in a Three-Phase System. *Sci. Rep.* **2016**, *6*, 35339.
(33) Hu, L.; Chen, M.; Fang, X.; Wu, L. Oil-water interfacial self-assembly: a novel strategy for nanofilm and nanodevice fabrication. *Chem. Soc. Rev.* **2012**, *41*, 1350−1362.
(34) Bourone, S. D.; Kaulen, C.; Homberger, M.; Simon, U. Directed Self-Assembly and Infrared Reflection Absorption Spectroscopy Analysis of Amphiphilic and Zwitterionic Janus Gold Nanoparticles. *Langmuir* **2016**, *32*, 954−962.
(35) Yang, G.; Hu, L.; Keiper, T. D.; Xiong, P.; Hallinan, D. T., Jr Gold Nanoparticle Monolayers with Tunable Optical and Electrical Properties. *Langmuir* **2016**, *32*, 4022−4033.
(36) Mahmoud, M. A. Tunable Plasmonic Neutral Density Filters and Chromatic Polarizers: Highly Packed 2D Arrays of Plasmonic Nanoparticle on Elastomer Substrate. *J. Phys. Chem. C* **2016**, *120*, 18249−18258.
(37) Hong, G. S.; Li, C.; Qi, L. M. Facile Fabrication of Two-Dimensionally Ordered Macroporous Silver Thin Films and Their Application in Molecular Sensing. *Adv. Funct. Mater.* **2010**, *20*, 3774−3783.
(38) Jiang, N.; Ruan, Q.; Qin, F.; Wang, J.; Lin, H. Q. Switching plasmon coupling through the formation of dimers from polyaniline-coated gold nanospheres. *Nanoscale* **2015**, *7*, 12516−12526.
(39) Shi, Q.; Si, K. J.; Sikdar, D.; Yap, L. W.; Premaratne, M.; Cheng, W. Two-Dimensional Bipyramid Plasmonic Nanoparticle Liquid Crystalline Superstructure with Four Distinct Orientational Packing Orders. *ACS Nano* **2016**, *10*, 967−976.
(40) Zhang, C.; You, E.; Jin, Q.; Yuan, Y.; Xu, M.; Ding, S.; Yao, J.; Tian, Z. Observing the dynamic ″hot spots″ on two-dimensional Au nanoparticles monolayer film. *Chem. Commun.* **2017**, *53*, 6788−6791.

DOI: 10.1021/acs.chemmater.7b05176
Chem. Mater. 2018, 30, 1989−1997